Results in Physics 59 (2024) 107560

Contents lists available at ScienceDirect

Results in Physics

journal homepage: www.elsevier.com/locate/rinp

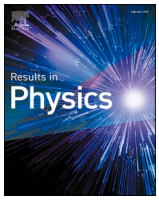

Two-dimensional ferromagnetic $V_2Cl_3Br_3$ with tunable topological phases

Wenjun Chen [a,1], Shiwei Zhang [a,1], Jiahang Li [a,1], Haopeng Zhang [b], Peng Wang [a], Liyu Hao [a,c], Tie Yang [a,*], Xingwen Tan [a,*]

[a] School of Physical Science and Technology, Southwest University, Chongqing 400715, China
[b] School of Science, Chongqing University of Posts and Telecommunications, Chongqing 400065, China
[c] Department of Technical Physics, School of Physics, Peking University, Beijing 100871, China

ARTICLE INFO

Keywords:
Nodal point state
Quantum anomalous Hall state
Topological phase
First principles calculation
Topological material
Density functional theory

ABSTRACT

In recent years, there has been significant research focus on topological states in two-dimensional materials, particularly those exhibiting intrinsic magnetic orderings. In this study, we employ theoretical calculations to uncover the remarkable band topology of monolayer $V_2Cl_3Br_3$. This two-dimensional compound not only possesses a half-metallic ferromagnetic ground state but also demonstrates exceptional thermodynamic and mechanical stabilities. Notably, we observe clean band crossings with complete spin polarization, which manifest as phase transitions between Weyl semimetal states and quantum anomalous Hall states under different magnetization directions. Both of these topological phases exhibit pronounced edge states. Furthermore, utilizing Monte Carlo simulations with the Heisenberg model, we estimate a high Curie temperature of up to 79.2 K, indicating its potential for spintronic development. Additionally, we analyze the mechanical properties of the material, emphasizing its isotropic mechanical behavior, which offers advantageous features for practical applications. These findings establish the foundation for further exploration of practical applications involving two-dimensional ferromagnetic topological states. Importantly, the identified material candidate can be readily incorporated into experimental preparation, thus accelerating progress in topological quantum applications and the development of half-metallic spintronic devices.

Introduction

The discovery of topological insulators has significantly enhanced our understanding of condensed matter physics [1–7]. In particular, the emergence of topological band theory has ushered in a new era of research in this field [8–16]. Topological states in crystalline materials are primarily determined by the intrinsic constraints of crystal symmetry. Notably, these states are often accompanied by nontrivial surface states, which exhibit exotic behavior beyond conventional bulk properties. Exploring the potential impact of these surface states on future quantum applications is a current focal point [17–28]. Both theoretical and experimental efforts have been devoted to this field, leading to a shift in focus from topological insulators to topological metals or semimetals [29–49]. In contrast to topological insulators, which possess a band gap in their bulk state, topological states in metals or semimetals are characterized by band crossings around the Fermi energy level. The resulting surface states, such as Fermi arcs or drumhead states, differ from the typical Dirac cone regime. Various topological elements can be defined based on their band degeneracies, dispersion types and orders, pseudospin structures, topological charges, and spatial configurations. These elements exhibit diverse properties that can be tailored for specific purposes [50,51]. The field of topological materials continues to witness significant progress, driven by the pursuit of understanding and harnessing their unique properties. The exploration of topological metals and semimetals, in particular, holds great promise for the development of novel quantum devices and applications [52].

With the continuous development, the concept of topology has extended beyond fermionic states to include bosonic states, such as phonons [53–58], photons [59–71] and magnons [72–75]. Among these bosonic states, phonons have garnered significant research attention as they represent another fundamental particle arising from lattice vibrations in solid-state systems, alongside electrons [58,76–80]. However, phononic bosons exhibit distinct properties compared to their fermionic counterparts [81–83]. Unlike electronic fermions, phononic states are

* Corresponding authors.
E-mail addresses: yangtie@swu.edu.cn (T. Yang), tanxingw@swu.edu.cn (X. Tan).
[1] Authors contribute equally to this work.

https://doi.org/10.1016/j.rinp.2024.107560
Received 16 January 2024; Received in revised form 1 March 2024; Accepted 8 March 2024
Available online 11 March 2024

not subject to the Pauli exclusion principle, and there is no spin–orbit coupling effect in the phononic system. The exploration of topological states has not been limited to three-dimensional materials but has also expanded to include two-dimensional materials, which have attracted considerable interest. Two-dimensional materials offer several practical advantages, including easy structural integration, compatibility with existing technologies, and straightforward device integration. Furthermore, topological states in two-dimensional magnetic materials hold great potential for spintronic applications. Similar to bulk materials, two-dimensional materials can exhibit diverse topological behaviors, discerned through considerations such as overlap band degeneracy, band dispersion conditions, and band crossing distributions [84–86]. The primary distinction in two-dimensional materials, stemming from their reduced dimensionality, lies in the transition from topological surface states to edge states. The investigation of topological phenomena in two-dimensional systems has opened up new avenues for understanding and manipulating emergent particles and their potential applications. This interdisciplinary exploration contributes to the advancement of fundamental physics and paves the way for innovative technologies in various fields [87–93].

Despite significant progress in the field, the range of identified topological properties and available material candidates in two-dimensional systems remains limited compared to their three-dimensional counterparts. Moreover, there have been few studies exploring magnetic configurations in this context. For instance, multiple nodal lines are revealed in the perfectly planar monolayer hexagonal indium carbide with the ferromagnetic ordering of spins and inclusion of spin–orbit coupling further enriches the magnetic and electronic properties [94]. Two spinful Weyl nodal lines have been discovered in a unique two-dimensional layered ferromagnetic electride Gd_2C and they further convert into multiple pairs of Weyl nodes through spin–orbit coupling [95]. Multiple time-reversal-breaking Weyl nodal lines have been found in the two-dimensional A_3C_2 (A = Ti, Zr, and Hf) ferromagnetic materials with high Curie temperature [96]. The discovery of twofold degenerate Weyl nodal lines in a single-layer gadolinium-silver compound has been demonstrated based on combined angle-resolved photoemission spectroscopy measurements and theoretical calculations [97]. The quantum anomalous Hall effect has been theoretically investigated in the monolayer Co_2Te material a with a sizable bandgap of 96 meV, characterized by the non-zero Chern number (C = 1) and a chiral edge state [98]. The coexistence of fully spin-polarized open/closed, and type-I/type-II/hybrid-type nodal lines have been theoretically identified in the half-metallic PrOBr monolayer [99]. Two topological nodal lines and one quadratic nodal point have been endowed in the two-dimensional Cr(II) five-membered heterocyclic metal organic frameworks [100]. Even with these advancements, there is an urgent need to explore and discover more two-dimensional magnetic topological materials, particularly those exhibiting clear and prominent topological states. In this study, we use theoretical calculations to propose the existence of ferromagnetic topological states in the monolayer ternary compound $V_2Cl_3Br_3$. This material not only possesses a half-metallic ferromagnetic ground state but also exhibits exceptional thermodynamic and mechanical stabilities. We identify a clean band crossing point in the spin-polarized electronic band structure, which undergoes a topological phase transition between Weyl nodal point and quantum anomalous Hall states when considering the spin–orbit coupling effect under different magnetization directions. Both topological phases exhibit distinct edge states, making them suitable for experimental detection and practical application. Furthermore, Monte Carlo simulations estimate a high Curie temperature of 79.2 K for $V_2Cl_3Br_3$, indicating its potential for spintronic development and application. Additionally, both elastic properties and isotropic mechanical behavior show advantageous features for practical applications. The proposed material candidates hold significant potential for related topological quantum applications and half-metallic spintronic development.

Computational methodology

In this study, we conducted a comprehensive investigation of the hexagonal monolayer $V_2Cl_3Br_3$ using first-principles calculations based on density functional theory (DFT) [101] within the VIENNA AB INITIO SIMULATION PACKAGE (VASP) [102]. The interactions between ionic cores and valence electrons were described using the projector augmented wave (PAW) method [103,104], considering the electronic configurations of V ($3d^4 4s^1$), Cl ($3s^2 3p^5$), and Br ($4s^2 4p^5$). The exchange and correlation interactions were treated using the generalized gradient approximation (GGA) of the Perdew-Burke-Ernzerhof (PBE) formalism [105]. To ensure accurate calculations, we employed periodic boundary conditions in the xy plane and added a large vacuum space of 15 Å along the z direction to prevent interference between layers. A cutoff energy of 500 eV was chosen for the planewave basis, and a Γ-centered Monkhorst-Pack k grid of $9 \times 9 \times 1$ was used to sample the Brillouin zone. Structural relaxation and self-consistent convergence were achieved by ensuring that the residual force per atom was less than 0.001 eV/Å and the total energy variation per atom was smaller than 1×10^{-6} eV. To assess the dynamic stability, we calculated the phonon spectra using density functional perturbation theory [106,107] implemented in the PHONOPY program [108]. The mechanical stability was investigated by determining the independent elastic constants using the stress–strain method [109] in the VASPKIT package [110]. In addition, we evaluated the thermal stability by performing ab initio molecular dynamics (AIMD) simulations in the canonical ensemble on a $4 \times 4 \times 1$ supercell [101,111]. For the electronic band structure, we considered the strong correlation interaction in the V transition metal element using the GGA + U approach [112] and also incorporated the spin–orbit coupling effect (SOC) [113] alongside the spin-polarized calculation. The calculation of topological edge states is based on a Wannier tight-binding Hamiltonian [114–116] constructed using the WANNIERTOOLS package [117].

Results and discussions

The monolayer $V_2Cl_3Br_3$ possesses a hexagonal lattice structure with space group P31m (No. 157), as illustrated in Fig. 1 a), in which the V atom is denoted by a red sphere, while the Cl and Br atoms are represented by green and brown spheres, respectively. Notably, the monolayer $V_2Cl_3Br_3$ exhibits a distinctive triple atomic layer arrangement, as observed in the side view of Fig. 1 a). This configuration consists of a vanadium planar layer situated between the top and bottom halide layers. The shaded region in the figure highlights the unit cell, which encompasses two equivalent V atoms and three equivalent Cl/Br atoms. In this structure, each V atom forms edge-sharing octahedra by bonding with three Cl and three Br atoms. Considering the propensity of the transition metal element V to exhibit magnetic behavior, we incorporated a spin-polarized condition in the two-dimensional system. Given the honeycomb structure formed by the V atoms, various magnetic configurations were explored, as shown in Fig. S1 of Supplementary Materials, including one ferromagnetic (FM) state and three antiferromagnetic (AFM) states: Néel antiferromagnetic (NAFM), stripe antiferromagnetic (SAFM), and zigzag antiferromagnetic (ZAFM). Calculation of the total energies revealed that the FM state possesses the lowest energy, with a difference of 1.22 eV compared to NAFM, 0.55 eV compared to SAFM, and 0.30 eV compared to ZAFM. Consequently, the FM configuration is determined to be the ground magnetic state. The lattice parameters of the monolayer $V_2Cl_3Br_3$ have been fully relaxed in the FM configuration, resulting in the values of a = b = 6.419 Å. To assess the stability of the obtained lattice structure, three key aspects have been thoroughly examined. Firstly, the dynamic stability was evaluated by analyzing the phonon dispersion spectrum, as depicted in Fig. 1 b). The absence of any imaginary frequencies confirms the dynamic stability of the monolayer $V_2Cl_3Br_3$, indicating that it does not exhibit any unstable vibrational modes. Secondly, the thermal stability

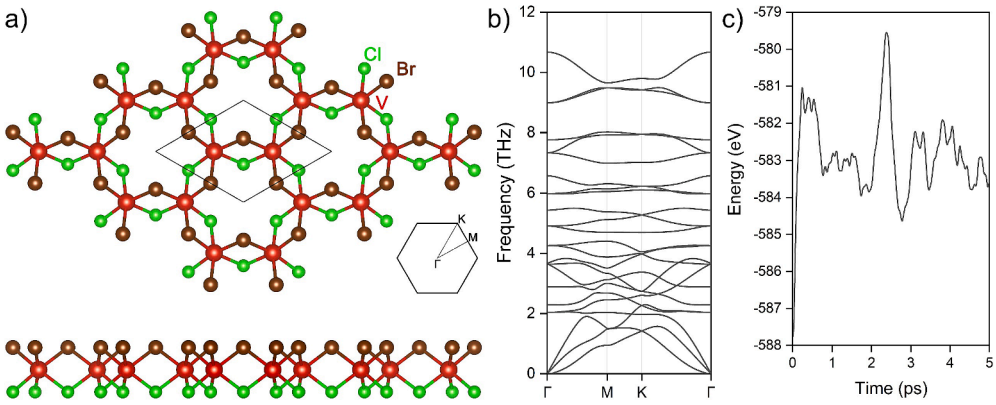

Fig. 1. The crystal structure a) of the monolayer $V_2Cl_3Br_3$ with both top and side views. The lattice unit cell is shown in the top view. The calculated phonon dispersion spectrum b) and the total energy fluctuations c) with time revolution under the AIMD simulations at 300 K.

was investigated through the AIMD simulations conducted for a duration of 5 ps at a temperature of 300 K. The small total energy variations throughout the simulation, as depicted in Fig. 1 c), further support the thermal stability of the system. Notably, these simulations revealed no structural disruptions or bond fractures, affirming the robustness of the crystal structure under thermal conditions. Furthermore, the mechanical stability of the monolayer $V_2Cl_3Br_3$ was assessed using the elastic stability criteria [118], which require $C_{11} > 0$ and $C_{11} > |C_{12}|$. The two independent elastic constants, C_{11} and C_{12}, were derived from the stress–strain method. Detailed lattice parameter and elastic constants are summarized in Table 1. The fulfillment of these stability criteria indicates the mechanical stability of the material. Collectively, the monolayer $V_2Cl_3Br_3$ exhibits remarkable stabilities from multiple perspectives, suggesting its high potential for experimental synthesis.

The spin-polarized electronic band structures of the monolayer $V_2Cl_3Br_3$ were computed using the fully relaxed crystal structures in the ground ferromagnetic state. The resulting band structures are presented in Fig. 2, where the recommended high symmetry points and paths were selected according to the VASPKIT program [110]. The band structure clearly exhibits a distinct half-metallic feature. In the spin-up channel, multiple bands intersect the Fermi level, indicating a metallic property. However, in the spin-down channel, a significant energy gap of 3.03 eV is observed, resembling an insulating characteristic. This intriguing half-metallic behavior of the monolayer $V_2Cl_3Br_3$ compound suggests the potential for achieving 100 % spin polarization of conduction electrons in the spin-up direction, rendering it highly compelling for spintronic applications. Furthermore, the presence of such a large half-metallic band gap is uncommon, particularly for non-oxide ferromagnetic monolayer materials. This attribute suggests potential resistance to thermal activation and lattice distortion [52]. Upon closer examination of the conducting conditions in the spin-up channel, a total of five bands are identified. Notably, two of these bands exhibit a linear crossing at the high symmetry point K around the Fermi energy level, as depicted in Fig. 2. This linear crossing point corresponds to topological nodal points, and based on the reverse dispersion slopes of the two bands, it falls into the Type-I nodal point state [119]. In consideration of the strong correlation effect inherent in the transition metal element V, the GGA + U method was also employed and the Hubbard U value of 3 eV has been applied. The calculation results in Fig. S2 of the Supplementary Materials demonstrate that the spin-polarized band structures and half-metallic behaviors, particularly the linear band crossing nodal point states in the spin-up channel, are accurately preserved.

In the preceding discussion, the impact of spin–orbit coupling (SOC) effect was not taken into account. To investigate its influence, the local band structures of the monolayer $V_2Cl_3Br_3$ around the Fermi level in the spin-up direction were examined by incorporating SOC in the calculations, considering the noncollinear magnetization direction. The obtained results are presented in Fig. 3. Different spontaneous magnetization directions were considered, specifically an in-plane direction [100] and an out-of-plane direction [0 0 1]. As depicted in Fig. 3, the band crossing remains unaffected under the in-plane magnetization [100] since this in-plane direction preserves the original M_y mirror symmetry. However, when the out-of-plane magnetization [0 0 1] is applied, the M_y symmetry is broken, resulting in a band gap at the band crossing point. This SOC-induced band gap is commonly observed in two-dimensional half-metallic materials. Notably, considering the involvement of the transition metal element V, the opened band gap of 30 meV is exceptionally small. Additionally, total energy calculations were performed under different magnetization directions. It was found that the energies within the in-plane magnetization directions are nearly identical and slightly higher (0.53 meV) than the out-of-plane [0 0 1] direction. This weak magnetic anisotropy suggests that the magnetism in the monolayer $V_2Cl_3Br_3$ is highly susceptible to external electric fields, allowing for easy manipulation of the magnetization direction through gating voltage. Moreover, from an application perspective, this perpendicular magnetic anisotropy holds significance for spintronic devices, particularly for multiple layer integration. Furthermore, by analyzing the spin density distribution and spin orbital decomposition, it was determined that the local bands around the Fermi level primarily arise from the *d* orbitals of V atoms, specifically the d_{xy}, d_{z^2}, and $d_{x^2-y^2}$ orbitals. Due to the substantially higher electronegativity of the halide elements, one valence electron of V is transferred to the halide Cl/Br, resulting in two unpaired electrons in each V atom within the formula unit. This configuration gives rise to a local magnetic moment on the V atom of 2.049 μ_B and a total magnetic moment of 3.792 μ_B for $V_2Cl_3Br_3$. Detailed magnetic properties, including total and partial magnetic moments, are summarized in Table 1.

Utilizing orbital decompositions in the low energy range around the Fermi level, a maximally localized Wannier tight-binding Hamiltonian was successfully constructed with the WANNIERTOOLS package. Based on this Wannier Hamiltonian model, the corresponding topological edge state of the monolayer $V_2Cl_3Br_3$ was examined. Specifically, the (1 0 0)

Table 1
The calculated structural lattices, mechanical constants and magnetic moments for the ferromagnetic monolayer $V_2Cl_3Br_3$.

a = b (Å)	C_{11} ($N{\cdot}M^{-1}$)	C_{12}	E	B	G	M_{total} μ_B	M_V	M_{Cl}	M_{Br}
6.419	53.91	18.56	47.52	36.23	17.68	3.792	2.049	−0.032	−0.042

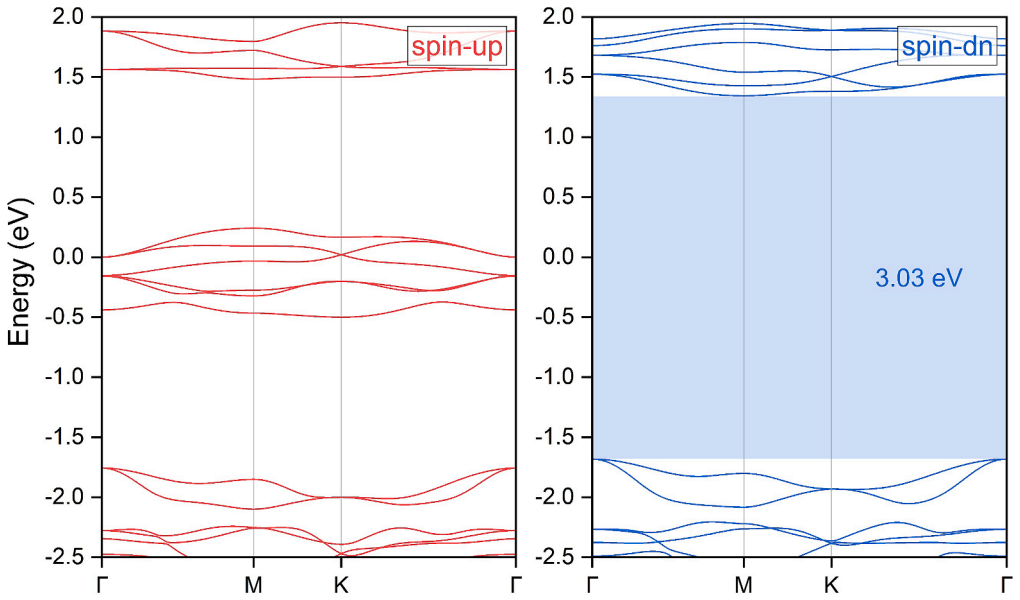

Fig. 2. The calculated electronic band structures of the monolayer $V_2Cl_3Br_3$. A large half metallic band gap of 3.03 eV present in the spin-down channel.

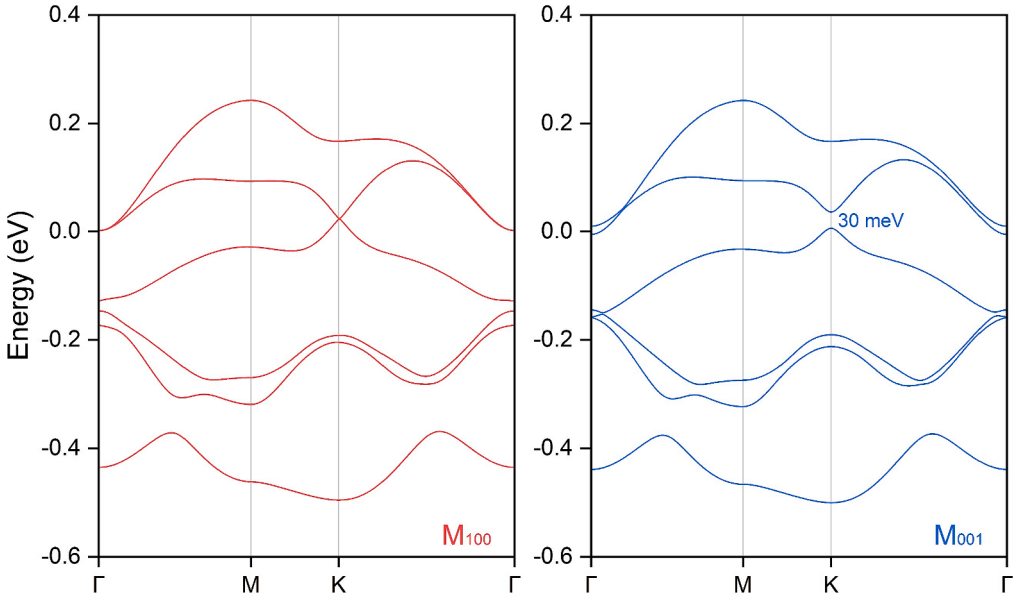

Fig. 3. The electronic band structures of the monolayer $V_2Cl_3Br_3$ with the consideration of the spin orbital coupling effect. Two different spontaneous magnetizations are applied, including the in-plane direction M_{100} and the out-of-plane direction M_{001}. The band crossing of the nodal point state can be maintained under the in-plane magnetizations, whereas a small band gap of 30 meV is opened up with the out-of-plane magnetization.

edge states were calculated and the results are presented in Fig. 4. Two magnetization directions, [100] and [001], were considered and labeled accordingly in the figures. To facilitate comparison, the same energy range and color scale were selected. For the in-plane [100] direction, a remarkable Fermi arc edge state was observed, precisely originating from the band crossing position of the nodal point. In contrast, for the out-of-plane [001] direction, a band gap opened up at the crossing point; however, a distinct chiral edge state connecting the valence and conduction bands could still be identified. This edge state, resulting from the SOC-induced gap, corresponds to the quantum anomalous Hall state. Several important features of the edge states should be noted. Firstly, the band structures exhibit high clarity, with the topological features easily distinguishable from the other trivial bands. Secondly, the edge states are well separated from other band projections, making them highly desirable for experimental detection and observation. Importantly, these ideal edge states with 100 % spin polarization are exceedingly rare, with only a few examples reported previously [120–126]. As mentioned earlier, the monolayer $V_2Cl_3Br_3$ compound exhibits soft magnetism that can be easily tuned by applying an external electric or magnetic field. Consequently, the topological phase transition between nodal point states and quantum anomalous Hall states can be readily achieved, with the phase switch requiring only a change in the direction of the applied field. Given the nearly identical spatial distributions and energy occupations of the two edge states, their phase transition provides an effective approach to investigate potential differences in the topological quantum behaviors between them.

In addition to the exceptional half metallicity and ideal topological properties discussed earlier, the thermal stability of magnetic ordering is crucial for practical advancements in spintronic devices, particularly in terms of withstanding thermal fluctuations during long term usage. To

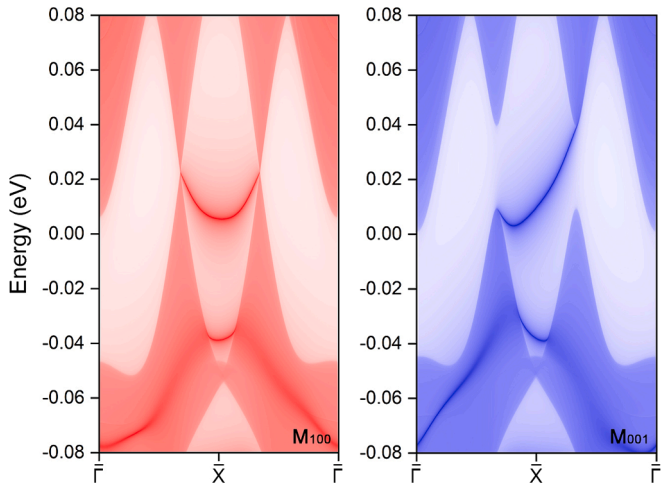

Fig. 4. The calculated edge states for the monolayer $V_2Cl_3Br_3$. Two magnetization orientations have been considered, namely the in-plane direction M_{100} and the out-of-plane direction M_{001}, as marked by the text.

assess this aspect, we conducted Monte Carlo simulations based on the Heisenberg model, employing the Metropolis algorithm to estimate the Curie temperature of the monolayer $V_2Cl_3Br_3$. By considering the third nearest neighbor as the maximum interaction range, we directly determined the coupling parameters of different magnetic ion pairs from the energy differences between various ferromagnetic (FM) and antiferromagnetic (AFM) configurations obtained through DFT calculations. Detailed values can be found in Table S1 of Supplementary Materials. To alleviate the constraints imposed by periodic boundaries, we constructed a 60×60 supercell of the monolayer $V_2Cl_3Br_3$ unit cell. At each temperature, the initial 1×10^5 steps were utilized for thermal equilibration, followed by averaging the subsequent 5×10^5 steps to gather the corresponding physical quantities. It is important to note that larger supercells, longer simulation periods, and more simulation points were tested and yielded highly similar results. To determine the Curie point, we calculated the magnetization and specific heat capacity, and their variations with temperature are presented in Fig. 5. The abrupt decrease in the average magnetic moment around 80 K signifies the phase transition from a ferromagnetic to a paramagnetic state. Utilizing the magnetic specific heat capacity, we obtained the precise Curie temperature for the monolayer $V_2Cl_3Br_3$ material as 79.2 K. Notably, this Curie temperature is remarkably high, particularly for two-dimensional systems, underscoring its promising potential for spintronic development and application.

In order to facilitate future experimental characterization and provide valuable insights for potential applications, we conducted a comprehensive evaluation of the mechanical properties of the monolayer $V_2Cl_3Br_3$. Several essential elastic parameters, including Young's modulus (E), bulk modulus (B), and shear modulus (G), were calculated and are reported in Table 1. It is worth noting that while the Young's modulus of the monolayer $V_2Cl_3Br_3$ is lower than that of graphene (340 $N{\cdot}m^{-1}$) and MoS_2 (128 $N{\cdot}m^{-1}$) [127,128], it remains comparable to phosphorene (23 $\sim$ 92 $N{\cdot}m^{-1}$) and silicene (60 $N{\cdot}m^{-1}$) [129,130]. Furthermore, the Poisson's ratio exhibits similarities to those of silicene and MoS_2 [131]. These findings indicate that the monolayer $V_2Cl_3Br_3$ possesses moderate rigidity against deformation and exhibits favorable mechanical properties. Additionally, we investigated the mechanical anisotropy of the monolayer $V_2Cl_3Br_3$ by analyzing the angle-dependent variations of Young's modulus and shear modulus, as depicted in Fig. 6. Our analysis reveals that the monolayer $V_2Cl_3Br_3$ demonstrates isotropic

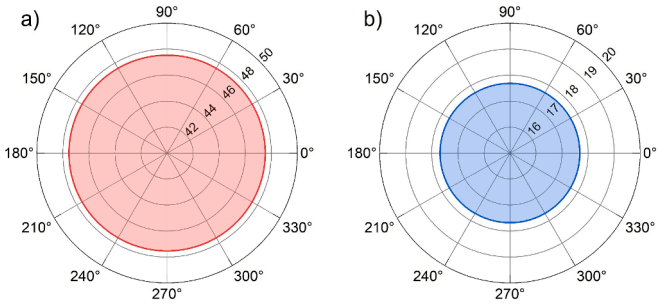

Fig. 6. The calculated angle-dependent variations of Young's modulus a) and shear modulus b) or the monolayer $V_2Cl_3Br_3$. The spherical distribution across all angles indicates the mechanical isotropy.

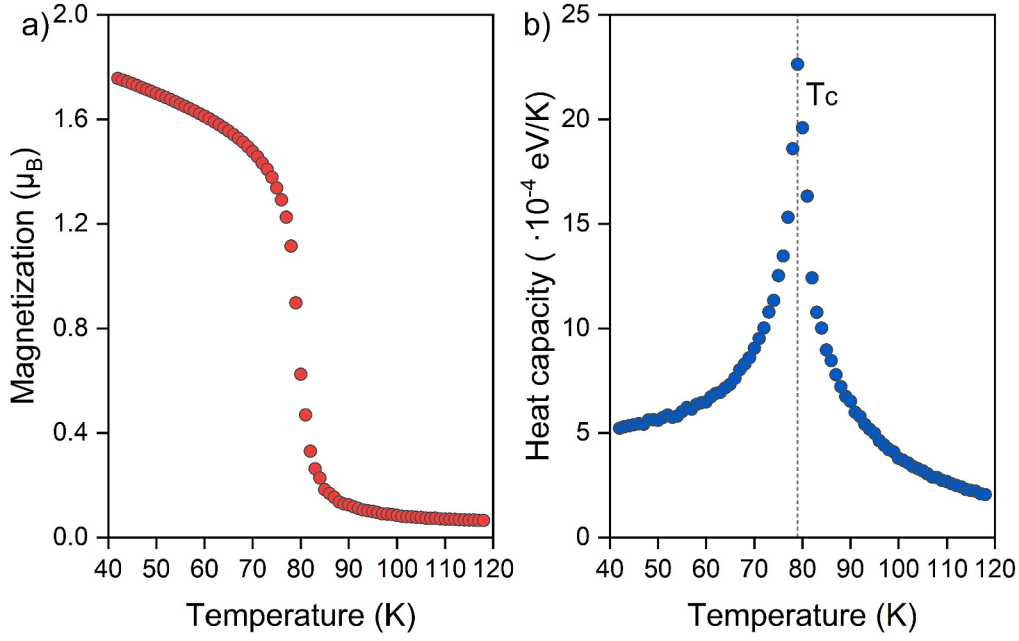

Fig. 5. The Monte Caro simulation results of the temperature dependent total magnetization a) and specific heat capacity b) for the monolayer $V_2Cl_3Br_3$. The obtained Curie temperature of 79.2 K is indicated by the dash line.

mechanical properties, with both Young's modulus and shear modulus exhibiting a uniform distribution across all angles. This isotropic mechanical behavior holds significant advantages for practical applications, particularly in terms of heterostructural combinations and integrations. For instance, when employing a two-dimensional material as a functional medium, the need for directional constraints is often present due to substrate support requirements. However, the mechanical isotropy observed in the monolayer $V_2Cl_3Br_3$ eliminates such constraints, offering enhanced flexibility in integration and design considerations.

Conclusions

This study presents a comprehensive investigation of the monolayer ternary compound $V_2Cl_3Br_3$, which exhibit both thermodynamic and mechanical stabilities. The electronic band structures of $V_2Cl_3Br_3$ exhibit remarkable half-metallic properties, featuring a substantial band gap in one spin direction and a Weyl nodal point in the other direction, resulting in a 100 % spin-polarized band topology. Considering the influence of spin–orbit coupling, the nodal point maintains its band crossing under in-plane magnetization direction, while transitioning into a quantum anomalous Hall state with an opened band gap under the out-of-plane direction. In both cases, distinct topological edge states are obtained, effectively separated from other trivial band projections, thus facilitating their experimental detection and observation. Furthermore, the magnetic behavior of $V_2Cl_3Br_3$ can be readily tuned by applying an external magnetic field, allowing for easy manipulation of the soft magnetism between different magnetization directions. These topological phase transformations provide an effective means to explore potential differences in topological quantum behaviors. In terms of practical application, the Curie temperature was estimated using Monte Carlo simulations, yielding a value of 79.2 K. This high Curie temperature demonstrates the promising potential of $V_2Cl_3Br_3$ for spintronic development and application. Additionally, various mechanical properties were derived, with particular emphasis on the isotropic mechanical behavior exhibited by $V_2Cl_3Br_3$. This isotropy is advantageous for practical applications, especially in terms of heterostructure combinations and substrate integrations. These promising findings lay a solid foundation for exploring the practical applications of ferromagnetic topological states in two-dimensional materials, particularly in the context of half-metallic developments and the integration of spintronic devices.

CRediT authorship contribution statement

Wenjun Chen: Investigation, Formal analysis, Data curation, Validation, Writing – original draft. **Shiwei Zhang:** Investigation, Formal analysis, Data curation, Validation, Writing – original draft. **Jiahang Li:** Investigation, Formal analysis, Data curation, Validation, Writing – original draft. **Haopeng Zhang:** Funding acquisition, Data curation, Visualization. **Peng Wang:** Software, Resources, Methodology, Validation. **Liyu Hao:** Data curation, Writing – review & editing. **Tie Yang:** Conceptualization, Methodology, Funding acquisition, Writing – review & editing. **Xingwen Tan:** Resources, Project administration, Supervision, Writing – review & editing.

Declaration of competing interest

The authors declare that they have no known competing financial interests or personal relationships that could have appeared to influence the work reported in this paper.

Data availability

Data will be made available on request.

Acknowledgments

This work was supported by the National Training Program of Innovation and Entrepreneurship for Undergraduates (No. 202310635046) and National Natural Science Foundation of China (No. 12304135). The authors wish to thank the high performance computing platform of School of Physical Science and Technology of Southwest University for the computational resources support.

Appendix A. Supplementary data

Supplementary data to this article can be found online at https://doi.org/10.1016/j.rinp.2024.107560.

References

[1] Ando Y, Fu L. Topological crystalline insulators and topological superconductors: from concepts to materials. Annu Rev Condens Matter Phys 2015;6:361–81.
[2] Vafek O, Vishwanath A. Dirac fermions in solids: From high-T-c cuprates and graphene to topological insulators and weyl semimetals, in: J.S. Langer (Ed.). Annu Rev Condens Matter Phys 2014;5:83–112.
[3] Moore JE. The birth of topological insulators. Nature 2010;464:194–8.
[4] Hasan MZ, Xu S-Y, Bian G. Topological insulators, topological superconductors and Weyl fermion semimetals: discoveries, perspectives and outlooks. Phys Scr 2015;T164:014001.
[5] Kruthoff J, de Boer J, van Wezel J, Kane CL, Slager R-J. Topological classification of crystalline insulators through band structure combinatorics. Phys Rev X 2017;7:041069.
[6] Hasan MZ, Kane CL. Colloquium: topological insulators. Rev Mod Phys 2010;82:3045–67.
[7] Qi X-L, Zhang S-C. Topological insulators and superconductors. Rev Mod Phys 2011;83:1057–110.
[8] Bansil A, Lin H, Das T. Colloquium: topological band theory. Rev Mod Phys 2016;88:021004.
[9] Regnault N, Xu Y, Li M-R, Ma D-S, Jovanovic M, Yazdani A, et al. Catalogue of flat-band stoichiometric materials. Nature 2022;603:824–8.
[10] Elcoro L, Wieder BJ, Song Z, Xu Y, Bradlyn B, Bernevig BA. Magnetic topological quantum chemistry. Nat Commun 2021;12:5965.
[11] Zhang T, Jiang Y, Song Z, Huang H, He Y, Fang Z, et al. Catalogue of topological electronic materials. Nature 2019;566:475–9.
[12] Bradlyn B, Elcoro L, Cano J, Vergniory MG, Wang Z, Felser C, et al. Topological quantum chemistry. Nature 2017;547:298–305.
[13] Xu Y, Elcoro L, Song Z-D, Wieder BJ, Vergniory MG, Regnault N, et al. High-throughput calculations of magnetic topological materials. Nature 2020;586:702–7.
[14] Narang P, Garcia CAC, Felser C. The topology of electronic band structures. Nat Mater 2021;20:293–300.
[15] Wieder BJ, Bradlyn B, Cano J, Wang Z, Vergniory MG, Elcoro L, et al. Topological materials discovery from crystal symmetry. Nat Rev Mater 2022;7:196–216.
[16] Xiao J, Yan B. First-principles calculations for topological quantum materials. Nat Rev Physics 2021;3:283–97.
[17] Po HC, Vishwanath A, Watanabe H. Complete theory of symmetry-based indicators of band topology. Nat Commun 2017;8:50.
[18] Tang F, Po HC, Vishwanath A, Wan X. Comprehensive search for topological materials using symmetry indicators. Nature 2019;566:486–9.
[19] Tang F, Po HC, Vishwanath A, Wan X. Efficient topological materials discovery using symmetry indicators. Nat Phys 2019;15:470–6.
[20] Corbae P, Ciocys S, Varjas D, Kennedy E, Zeltmann S, Molina-Ruiz M, et al. Observation of spin-momentum locked surface states in amorphous Bi_2Se_3. Nat Mater 2023;22:200–6.
[21] He B, Wang Y, Arguilla MQ, Cultrara ND, Scudder MR, Goldberger JE, et al. The Fermi surface geometrical origin of axis-dependent conduction polarity in layered materials. Nat Mater 2019;18:568–72.
[22] Liu ZK, Yang LX, Sun Y, Zhang T, Peng H, Yang HF, et al. Evolution of the Fermi surface of Weyl semimetals in the transition metal pnictide family. Nat Mater 2016;15:27–31.
[23] Medjanik K, Fedchenko O, Chernov S, Kutnyakhov D, Ellguth M, Oelsner A, et al. Direct 3D mapping of the Fermi surface and Fermi velocity. Nat Mater 2017;16:615–21.
[24] Kim D, Cho S, Butch NP, Syers P, Kirshenbaum K, Adam S, et al. Surface conduction of topological Dirac electrons in bulk insulating Bi_2Se_3. Nat Phys 2012;8:459–63.
[25] Belopolski I, Manna K, Sanchez DS, Chang G, Ernst B, Yin J, et al. Discovery of topological Weyl fermion lines and drumhead surface states in a room temperature magnet. Science 2019;365:1278–81.
[26] Morali N, Batabyal R, Nag PK, Liu E, Xu Q, Sun Y, et al. Fermi-arc diversity on surface terminations of the magnetic Weyl semimetal $Co_3Sn_2S_2$. Science 2019;365:1286–91.
[27] Xu S-Y, Liu C, Kushwaha SK, Sankar R, Krizan JW, Belopolski I, et al. Observation of Fermi arc surface states in a topological metal. Science 2015;347:294.

[28] Yang T, Kuang M-Q, Zhang X, Wu W, Yu Z-M. Intrinsic topological property for precise structure differentiation. Phys Rev B 2023;107:155138.
[29] Yan B, Felser C. Topological materials: Weyl semimetals. Annu Rev Condens Matter Phys 2017;8:337–54.
[30] Gao H, Venderbos JWF, Kim Y, Rappe AM. Topological semimetals from first principles. Annu Rev Mat Res 2019;49:153–83.
[31] Schoop LM, Pielnhofer F, Lotsch BV. Chemical principles of topological semimetals. Chem Mater 2018;30:3155–76.
[32] Fang C, Weng H, Dai X, Fang Z. Topological nodal line semimetals. Chinese Phys B 2016;25:117106.
[33] Feng X, Zhu J, Wu W, Yang SA. Two-dimensional topological semimetals*. Chinese Phys B 2021;30:107304.
[34] Yu R, Fang Z, Dai X, Weng H. Topological nodal line semimetals predicted from first-principles calculations. Front Phys 2017;12:127202.
[35] Li J, Zhang Z, Wang C, Huang H, Gu B-L, Duan W. Topological semimetals from the perspective of first-principles calculations. J Appl Phys 2020;128:191101.
[36] Weng H, Dai X, Fang Z. Topological semimetals predicted from first-principles calculations. J Phys-Condens Matter 2016;28:303001.
[37] Hirayama M, Okugawa R, Murakami S. Topological semimetals studied by ab initio calculations. J Phys Soc Jpn 2018;87:041002.
[38] Wang KL, Wu Y, Eckberg C, Yin G, Pan Q. Topological quantum materials. MRS Bull 2020;45:373–9.
[39] Burkov AA. Topological semimetals. Nat Mater 2016;15:1145–8.
[40] Jia S, Xu S-Y, Hasan MZ. Weyl semimetals, Fermi arcs and chiral anomalies. Nat Mater 2016;15:1140–4.
[41] Bernevig BA. It's been a Weyl coming. Nat Phys 2015;11:698–9.
[42] Shao Y, Rudenko AN, Hu J, Sun Z, Zhu Y, Moon S, et al. Electronic correlations in nodal-line semimetals. Nat Phys 2020;16:636–41.
[43] Jin L, Zhang X, Liu Y, Dai X, Shen X, Wang L, et al. Two-dimensional Weyl nodal-line semimetal in a d(0) ferromagnetic K_2N monolayer with a high Curie temperature. Phys Rev B 2020;102:125118.
[44] He T, Zhang X, Liu Y, Dai X, Liu G, Yu Z-M, et al. Ferromagnetic hybrid nodal loop and switchable type-I and type-II Weyl fermions in two dimensions. Phys Rev B 2020;102:075133.
[45] Zhang X, Wang X, He T, Wang L, Yu W-W, Liu Y, et al. Magnetic topological materials in two-dimensional: theory, material realization and application prospects. Sci Bull 2023;68:2639–57.
[46] Yang T, Jin L, Liu Y, Zhang X, Wang X. Spin-polarized type-II nodal loop and nodal surface states in hexagonal compounds $XTiO_2$ (X = Li, Na, K, Rb). Phys Rev B 2021;103:235140.
[47] Zhang H, Wang P, Hao L, Wu Z, Wu W, Cheng Z, et al. Ferromagnetic topological states in monolayer vanadium halides toward heterostructure applications. Apl Mater 2024;12:011119.
[48] Zhang N, Ding X, Zhan F, Li H, Li H, Tang K, et al. Temperature-dependent and magnetism-controlled Fermi surface changes in magnetic Weyl semimetals. Phys Rev Res 2023;5:L022013.
[49] Ning Z, Ding X, Xu D-H, Wang R. Robustness of half-integer quantized Hall conductivity against disorder in an anisotropic Dirac semimetal with parity anomaly. Phys Rev B 2023;108:L041104.
[50] Yu Z, Zhang Z, Liu G-B, Wu W, Li X-P, Zhang R-W, et al. Encyclopedia of emergent particles in three-dimensional crystals. Sci Bull 2021;67:375.
[51] Zhou F, Guangqian D, Zhenxiang C, Gokhan S, Hong C, Xiaotian W. Pnma metal hydride system LiBH: a superior topological semimetal with the coexistence of twofold and quadruple degenerate topological nodal lines. J Phys-Condens Matter 2020;32:365502.
[52] Jin K-H, Jiang W, Sethi G, Liu F. Topological quantum devices: a review. Nanoscale 2023;15:12787–817.
[53] Liu Y, Chen X, Xu Y. Topological phononics: from fundamental models to real materials. Adv Funct Mater 2020;30:1904784.
[54] Wang P, Lu L, Bertoldi K. Topological phononic crystals with one-way elastic edge waves. Phys Rev Lett 2015;115:104302.
[55] Süsstrunk R, Huber SD. Observation of phononic helical edge states in a mechanical topological insulator. Science 2015;349:47–50.
[56] Huber SD. Topological mechanics. Nat Phys 2016;12:621–3.
[57] Stenull O, Kane CL, Lubensky TC. Topological Phonons and Weyl Lines in Three Dimensions. Phys Rev Lett 2016;117:068001.
[58] Yang T, Gao Y, Hao L, Zhang H, Tan X, Wang P, et al. Cladded phononic nodal frame state in biatomic alkali-metal sulfides. Phys Rev B 2023;108:134310.
[59] Yang B, Guo Q, Tremain B, Liu R, Barr LE, Yan Q, et al. Ideal Weyl points and helicoid surface states in artificial photonic crystal structures. Science 2018;359:1013–6.
[60] Liu F, Deng H-Y, Wakabayashi K. Topological photonic crystals with zero Berry curvature. Phys Rev B 2018;97:035442.
[61] Wang H, Gupta SK, Xie B, Lu M. Topological photonic crystals: a review. Front Optoelectron 2020;13:50–72.
[62] Xu H, Zhou J, Wang H, Li J. Giant photonic response of Mexican-hat topological semiconductors for mid-infrared to terahertz applications. J Phys Chem Lett 2020;11:6119–26.
[63] Deng W-M, Chen Z-M, Li M-Y, Guo C-H, Tian Z-T, Sun K-X, et al. Ideal nodal rings of one-dimensional photonic crystals in the visible region. Light Sci Appl 2022;11:134.
[64] Wang H, Tang G, He Y, Wang Z, Li X, Sun L, et al. Ultracompact topological photonic switch based on valley-vortex-enhanced high-efficiency phase shift. Light Sci Appl 2022;11:292.
[65] Park H, Gao W, Zhang X, Oh SS. Nodal lines in momentum space: topological invariants and recent realizations in photonic and other systems. Nanophotonics 2022;11:2779–801.
[66] Stützer S, Plotnik Y, Lumer Y, Titum P, Lindner NH, Segev M, et al. Photonic topological Anderson insulators. Nature 2018;560:461–5.
[67] Pan Y, Cui C, Chen Q, Chen F, Zhang L, Ren Y, et al. Real higher-order Weyl photonic crystal. Nat Commun 2023;14:6636.
[68] Xie B, Su G, Wang H-F, Liu F, Hu L, Yu S-Y, et al. Higher-order quantum spin Hall effect in a photonic crystal. Nat Commun 2020;11:3768.
[69] Lin Z-K, Wang Q, Liu Y, Xue H, Zhang B, Chong Y, et al. Topological phenomena at defects in acoustic, photonic and solid-state lattices. Nat Rev Phys 2023;5:483–95.
[70] Zhang H, Sui W, Zhang Y, Liu G, Shi Q, Lv Z, Zhang D, Rong C, Yang B. Disorder-driven collapse of topological phases in photonic topological insulator. Phys Status Solidi B 2022;259:2200214.
[71] Raghu S, Haldane FDM. Analogs of quantum-Hall-effect edge states in photonic crystals. Phys Rev A 2008;78:033834.
[72] Li K, Li C, Hu J, Li Y, Fang C. Dirac and nodal line magnons in three-dimensional antiferromagnets. Phys Rev Lett 2017;119:247202.
[73] Bao S, Gu Z-L, Shangguan Y, Huang Z, Liao J, Zhao X, et al. Direct observation of topological magnon polarons in a multiferroic material. Nat Commun 2023;14:6093.
[74] Corticelli A, Moessner R, McClarty PA. Spin-space groups and magnon band topology. Phys Rev B 2022;105:064430.
[75] Zhu F, Zhang L, Wang X, Santos FJd, Song J, Mueller T, Schmalzl K, Schmidt WF, Ivanov A, Park JT, Xu J, Ma J, Lounis S, Blügel S, Mokrousov Y, Su Y, Brückel T. Topological magnon insulators in two-dimensional van der Waals ferromagnets $CrSiTe_3$ and $CrGeTe_3$: toward intrinsic gap-tunability. Sci Adv 2021;7:eabi7532.
[76] Liu Y, Xu Y, Duan W. Berry phase and topological effects of phonons. Natl Sci Rev 2018;5:314–6.
[77] Mousavi SH, Khanikaev AB, Wang Z. Topologically protected elastic waves in phononic metamaterials. Nat Commun 2015;6:8682.
[78] He C, Ni X, Ge H, Sun X-C, Chen Y-B, Lu M-H, et al. Acoustic topological insulator and robust one-way sound transport. Nat Phys 2016;12:1124–9.
[79] Xie C, Yuan H, Liu Y, Wang X. Two-nodal surface phonons in solid-state materials. Phys Rev B 2022;105:054307.
[80] Süsstrunk R, Huber SD. Classification of topological phonons in linear mechanical metamaterials. Proc Natl Acad Sci 2016;113:E4767–75.
[81] Li J, Liu J, Baronett SA, Liu M, Wang L, Li R, et al. Computation and data driven discovery of topological phononic materials. Nat Commun 2021;12:1204.
[82] Liu Q-B, Qian Y, Fu H-H, Wang Z. Symmetry-enforced Weyl phonons. NPJ Comput Mater 2020;6:95.
[83] Zhang S-B, Zhou J. Quantum oscillations in acoustic phonons in Weyl semimetals. Phys Rev B 2020;101:085202.
[84] Yang T, Zhou J, Song TT, Shen L, Feng YP, Yang M. High-throughput identification of exfoliable two-dimensional materials with active basal planes for hydrogen evolution. ACS Energy Lett 2020;5:2313–21.
[85] Nan-Shu L, Cong W, Wei J. Recent research advances in two-dimensional magnetic materials. Acta Phys Sin 2022;71:127504.
[86] Miró P, Audiffred M, Heine T. An atlas of two-dimensional materials. Chem Soc Rev 2014;43:6537–54.
[87] Wang L, Zhao M, Wang J, Liu Y, Liu G, Wang X, et al. High-performance hydrogen evolution reaction catalysts in two-dimensional nodal line semimetals. ACS Appl Mater Interfaces 2023;15:51225–30.
[88] Zhang X, Jin L, Dai X, Chen G, Liu G. Two-dimensional GaN: an excellent electrode material providing fast ion diffusion and high storage capacity for Li-Ion and Na-Ion batteries. ACS Appl Mater Interfaces 2018;10:38978–84.
[89] Chen H, Zhang S, Jiang W, Zhang C, Guo H, Liu Z, et al. Prediction of two-dimensional nodal-line semimetals in a carbon nitride covalent network. J Mater Chem A 2018;6:11252–9.
[90] Meng W, Zhang X, Liu Y, Dai X, Gao H, Liu G. Two-dimensional $[CaCl]^{+}\cdot e^{-}$ with its strippable feasibility as an applicable electride with room-temperature ferromagnetism and extremely low work function. J Mater Chem C 2021;9:15477–87.
[91] Zhang S, Wu H, Yang L, Zhang G, Xie Y, Zhang L, et al. Two-dimensional magnetic atomic crystals. Mater Horiz 2022;9:559–76.
[92] Ashton M, Gluhovic D, Sinnott SB, Guo J, Stewart DA, Hennig RG. Two-dimensional intrinsic half-metals with large spin gaps. Nano Lett 2017;17:5251–7.
[93] Mounet N, Gibertini M, Schwaller P, Campi D, Merkys A, Marrazzo A, et al. Two-dimensional materials from high-throughput computational exfoliation of experimentally known compounds. Nat Nanotechnol 2018;13:246–52.
[94] Jeon S, Oh Y-T, Kim Y. Ferromagnetic nodal-line metal in monolayer h-InC. Phys Rev B 2019;100:035406.
[95] Liu S, Wang C, Liu L, Choi J-H, Kim H-J, Jia Y, et al. Ferromagnetic Weyl fermions in two-dimensional layered electride Gd_2C. Phys Rev Lett 2020;125:187203.
[96] Zhou F, Liu Y, Kuang M, Wang P, Wang J, Yang T, et al. Time-reversal-breaking Weyl nodal lines in two-dimensional A_3C_2 (A = Ti, Zr, and Hf) intrinsically ferromagnetic materials with high Curie temperature. Nanoscale 2021;13:8235–41.
[97] Feng B, Zhang R-W, Feng Y, Fu B, Wu S, Miyamoto K, et al. Discovery of Weyl nodal lines in a single-layer ferromagnet. Phys Rev Lett 2019;123:116401.
[98] Liu Y-S, Sun H, Hu C-S, Wu Y-J, Zhang C-W. First-principles prediction of quantum anomalous Hall effect in two-dimensional Co_2Te lattice. Chinese Phys B 2023;32:027101.

[99] Jin L, Zhang X, Liu Y, Dai X, Liu G. Theoretical realization of two-dimensional half-metallicity and fully spin-polarized multiple nodal-line fermions in monolayer PrOBr. Phys Rev B 2022;105:075414.
[100] Li X, Liu Q-B, Tang Y, Li W, Ding N, Liu Z, et al. Quintuple function integration in two-dimensional Cr(II) five-membered heterocyclic metal organic frameworks via tuning ligand spin and lattice symmetry. J Am Chem Soc 2023;145:7869–78.
[101] Payne MC, Teter MP, Allan DC, Arias TA, Joannopoulos JD. Iterative minimization techniques forab initiototal-energy calculations: molecular dynamics and conjugate gradients. Rev Mod Phys 1992;64:1045–97.
[102] Hafner J. Ab-initio simulations of materials using VASP: Density-functional theory and beyond. J Comput Chem 2008;29:2044–78.
[103] Kresse G, Joubert D. From ultrasoft pseudopotentials to the projector augmented-wave method. Phys Rev B 1999;59:1758–75.
[104] Blöchl PE. Projector augmented-wave method. Phys Rev B 1994;50:17953–79.
[105] Perdew JP, Burke K, Ernzerhof M. Generalized gradient approximation made simple. Phys Rev Lett 1996;77:3865–8.
[106] Gonze X, Lee C. Dynamical matrices, Born effective charges, dielectric permittivity tensors, and interatomic force constants from density-functional perturbation theory. Phys Rev B 1997;55:10355–68.
[107] Giannozzi P, de Gironcoli S, Pavone P, Baroni S. Ab initio calculation of phonon dispersions in semiconductors. Phys Rev B 1991;43:7231–42.
[108] Togo A, Tanaka I. First principles phonon calculations in materials science. Scr Mater 2015;108:1–5.
[109] Wang J, Li J, Yip S, Phillpot S, Wolf D. Mechanical instabilities of homogeneous crystals. Phys Rev B Condens Matter 1995;52:12627–35.
[110] Wang V, Xu N, Liu J-C, Tang G, Geng W-T. VASPKIT: a user-friendly interface facilitating high-throughput computing and analysis using VASP code. Comput Phys Commun 2021;267:108033.
[111] Bucher D, Pierce LCT, McCammon JA, Markwick PRL. On the use of accelerated molecular dynamics to enhance configurational sampling in ab initio simulations. J Chem Theory Comput 2011;7:890–7.
[112] Dudarev SL, Botton GA, Savrasov SY, Humphreys CJ, Sutton AP. Electron-energy-loss spectra and the structural stability of nickel oxide: an LSDA+U study. Phys Rev B 1998;57:1505–9.
[113] Kresse G, Furthmüller J. Efficient iterative schemes for ab initio total-energy calculations using a plane-wave basis set. Phys Rev B 1996;54:11169–86.
[114] Marzari N, Vanderbilt D. Maximally localized generalized Wannier functions for composite energy bands. Phys Rev B 1997;56:12847–65.
[115] Mostofi AA, Yates JR, Pizzi G, Lee Y-S, Souza I, Vanderbilt D, et al. An updated version of wannier90: a tool for obtaining maximally-localised Wannier functions. Comput Phys Commun 2014;185:2309–10.
[116] Mostofi AA, Yates JR, Lee Y-S, Souza I, Vanderbilt D, Marzari N. wannier90: A tool for obtaining maximally-localised Wannier functions. Comput Phys Commun 2008;178:685–99.
[117] Wu Q, Zhang S, Song H-F, Troyer M, Soluyanov AA. WannierTools: an open-source software package for novel topological materials. Comput Phys Commun 2018;224:405–16.
[118] Mouhat F, Coudert FX. Necessary and sufficient elastic stability conditions in various crystal systems. Phys Rev B 2014;90:224104.
[119] Zheng B, Xia B, Wang R, Chen Z, Zhao J, Zhao Y, et al. Ideal type-III nodal-ring phonons. Phys Rev B 2020;101:100303.
[120] Liu Z, Feng W, Xin H, Gao Y, Liu P, Yao Y, et al. Two-dimensional spin–valley-coupled Dirac semimetals in functionalized SbAs monolayers. Mater Horiz 2019;6:781–7.
[121] Sun Q, Ma Y, Kioussis N. Two-dimensional Dirac spin-gapless semiconductors with tunable perpendicular magnetic anisotropy and a robust quantum anomalous Hall effect. Mater Horiz 2020;7:2071–7.
[122] Gong J, Ding G, Xie C, Wang W, Liu Y, Zhang G, Wang X. Genuine Dirac half-metals in two-dimensions. Adv Sci 2023:2307297.
[123] Wang L, Jin L, Liu G, Liu Y, Dai X, Zhang X. Theoretical realization of two-dimensional Dirac/Weyl line-node and traversing edge states in penta-X2Y monolayers. Appl Mater Today 2021;23:101057.
[124] Jin L, Zhang X, He T, Meng W, Dai X, Liu G. Ferromagnetic two-dimensional metal-chlorides MCl (M = Sc, Y, and La): Candidates for Weyl nodal line semimetals with small spin-orbit coupling gaps. Appl Surf Sci 2020;520:146376.
[125] Wu M-X, Wang P, Yang T, Kuang A-L, Kuang M-Q, Yuan H-K. Possible topological states in two dimensional Kagome ferromagnet MnGe. J Alloy Compd 2022;907:164389.
[126] Liu J, Liu Z, Song T, Cui X. Computational search for two-dimensional intrinsic half-metals in transition-metal dinitrides. J Mater Chem C 2017;5:727–32.
[127] Cai Y, Zhang G, Zhang Y-W. Polarity-reversed robust carrier mobility in monolayer MoS_2 nanoribbons. J Am Chem Soc 2014;136:6269–75.
[128] Lee C, Wei X, Kysar JW, Hone J. Measurement of the elastic properties and intrinsic strength of monolayer graphene. Science 2008;321:385–8.
[129] Wang L, Kutana A, Zou X, Yakobson BI. Electro-mechanical anisotropy of phosphorene. Nanoscale 2015;7:9746–51.
[130] McGuire MA. Crystal and magnetic structures in layered, transition metal dihalides and trihalides. Crystals 2017;7:121.
[131] Akinwande D, Brennan CJ, Bunch JS, Egberts P, Felts JR, Gao H, et al. A review on mechanics and mechanical properties of 2D materials—Graphene and beyond. Extreme Mech Lett 2017;13:42–77.